Advanced Journal of Chemistry-Section A

Journal homepage: www.ajchem-a.com

Original Research Article

Impact of Annealing Temperature on Lanthanum Erbium Telluride ($La_{0.1}Er_{0.2}Te_{0.2}$) Nanoparticles Synthesized *via* Hydrothermal Approach

Haneef Shah[1,2], Shahbaz Afzal[1,2], Mohammad Usman[1], Kamran Shahzad[3], Imosobomeh Lucky Ikhioya[2,4]*

[1] *Department of Physics, University of Education Lahore, DG Khan Campus, Punjab, Pakistan*
[2] *National Centre for Physics, Quaid-i-Azam University Campus, Islamabad, Pakistan*
[3] *Department of Physics, International Islamic University Islamabad, Islamabad, Pakistan*
[4] *Department of Physics and Astronomy, University of Nigeria Nsukka, Nsukka, Nigeria*

ARTICLE INFO

Article history

Submitted: 16 July 2023
Revised: 09 August 2023
Accepted: 13 August 2023
Available online: 13 August 2023
Manuscript ID: AJCA-2305-1386
Checked for Plagiarism: Yes

DOI: **10.22034/AJCA.2023.407424.1386**

KEYWORDS

Rear earth element
Lanthanum
Erbium
Telluride
nanoparticles

ABSTRACT

In this study, we synthesized $La_{0.1}Er_{0.2}Te_{0.2}$ nanoparticle using 0.2 mol of $Er(NO_3)_3{\cdot}5H_2O$, 0.1 mol of $La(NO_3)_3{\cdot}6H_2O$, and 0.2 mol of $Te(NO_3)_4$ through hydrothermal and doctor blade methods. The $La_{0.1}Er_{0.2}Te_{0.2}$ material reveals a hexagonal structure corresponding to a 2theta angle of 13.263°. 15.375°. 16.943°. 18.924°. 25.788°. and 27.356° for $La_{0.1}Er_{0.2}Te_{0.2}$ unannealed and 13.302°, 15.489°, 16.960°, 19.055°, 25.862°, and 27.373° for annealed samples. The XRD pattern showed that the crystallinity increased with higher annealing temperature. Unannealed $La_{0.1}Er_{0.2}Te_{0.2}$ had glow-like nanoparticles. The $La_{0.1}Er_{0.2}Te_{0.2}$ nanoparticles showed high absorbance in the visible area of the spectra with 0.648 a.u. The absorbance of the material decreased as the annealing temperature increased. The higher the annealing temperature, the lower the absorbance of the material. The unannealed nanoparticle has a bandgap energy of 3.50 eV. The annealing nanoparticles have a bandgap of 3.27 to 2.26 eV. The higher the annealing temperature, the lower the bandgap of the material.

GRAPHICAL ABSTRACT

* Corresponding author: Ikhioya, Imosobomeh Lucky
✉ E-mail: imosobomeh.ikhioya@unn.edu.ng
© 2023 by SPC (Sami Publishing Company)

Introduction

The periodic table comprises a group of elements that are known as rare earth elements, containing lanthanum (La) and erbium (Er) which are a part of the lanthanide series. The rare earth elements (REEs) are categorized into light and heavy groups. REEs are categorized by atomic number and weight. The two groups known are the heavy rare earth elements and light rare earth elements. The ten heavy rare earth elements are ytterbium, erbium, terbium, dysprosium, holmium, gadolinium, lutetium, europium, thulium, and yttrium [1]. The light rare earth elements include cerium, praseodymium, lanthanum, neodymium, promethium, and samarium. Wind turbines, LED light bulbs, TV, cell phones, computers, memory, and solar panels rely on REEs. All high-tech devices contain these crucial elements. Flat-panel televisions use all REE. Smart batteries used in hybrid vehicles and to power all-electric often contain various REE compounds. These elements offer reduced energy consumption, increased efficiency, smaller size, faster speed, extended durability, and heat resistance. Demand for green technology has increased in recent years [2]. Analytical instruments are becoming smaller and more efficient with the help of these technologies.

Rare earth luminous materials have a wide range of applications in different fields. They can be used for industrial such as metal and glass production. Rare earth nano-powder added to epoxy resin improved toughness, high-temperature resistance, and strength. It also improved overall performance with a small amount of material and low cost [3]. Organic silicon materials can have increased high-temperature resistance and ultraviolet resistance. Lanthanum erbium telluride (LaErTe) nanomaterials resist high temperatures, radiation, and ultraviolet light. LaErTe ions are used for high-energy detectors. These scintillators can be used in many ways to detect cosmic rays in biomedical tests.

LaErTe nanomaterials have high capacitance than other transition metal oxides. The nanomaterials have good conductivity, large surface area, and strong cycle stability [4,5]. Changing the form and size of rare-earth nanomaterials can increase their electronic conductivity. The nanostructuring of LaErTe material increases surface area [4-6]. The shape exposes active sites and high-energy crystal planes, giving the material a longer cycle life. Mixing rare earths with other transition metal chalcogenides can improve pseudo-capacitance and cycle efficiency [6-11]. Distinct properties and structures are found in rare earth elements. Rare earth-based nanomaterials have gained attention due to their environmentally safe qualities and exceptional redox capabilities. There are various techniques available for synthesizing rare-earth-based nanomaterials, including Hydrothermal, electrodeposition [12–20], thermal decomposition, micro-emulsion method, atomic layer deposition, thermal oxidation, sonication, sputtering, electrochemistry, physical vapor deposition, and combustion methods, which are ecologically safe, cost-effective, and straightforward [1,9]. Hydrothermal synthesis is considered one of the most crucial and well-established processes for nonmaterial synthesis due to its effectiveness and reliability [1,3,6,9]. This process uses an enclosed and heated device, like an autoclave or bomb calorimeter, and involves chemical reactions using water as a solvent.

In this study, we use hydrothermal technique to synthesize the nanoparticle of lanthanum erbium telluride ($La_{0.1}Er_{0.2}Te_{0.2}$) using 0.2 mol of $Er(NO_3)_3{\cdot}5H_2O$, 0.1 mol of $La(NO_3)_3{\cdot}6H_2O$, and 0.2 mol of $Te(NO_3)_4$ and study the impact of annealing temperature on the structural, optical, morphological, and electrical features of the material.

Experimental Details

Materials

The materials used in this work include lanthanum nitrate hexahydrate ($La(NO_3)_3 \cdot 6 H_2O$) Sigma-Aldrich 99.9%, erbium trinitrate pentahydrate ($Er(NO_3)_3 \cdot 5H2O$) Sigma-Aldrich 99.9%, tellurium nitrate ($Te(NO_3)_4$), distilled water, heating mantle, power source, Multimeter, fluorine-doped tin oxide as the substrate (FTO), thermostatic blast resettable oven within a temperature range of 50 °C - 1000 °C.

Synthesis of lanthanum erbium telluride ($La_{0.1}Er_{0.2}Te_{0.2}$)

Lanthanum erbium telluride ($La_{0.1}Er_{0.2}Te_{0.2}$) was prepared using the hydrothermal technique. 25 mL of water was used to dissolve 0.2 mol of erbium trinitrate pentahydrate ($Er(NO_3)_3 \cdot 5H2O$) and 0.1 mol of lanthanum nitrate hexahydrate ($La(NO_3)_3 \cdot 6H_2O$) and thoroughly stirred to get a homogeneous solution. The FTO substrate was repeatedly sterilized in distilled water and ethanol before usage. 0.2 mol of tellurium nitrate ($Te(NO_3)_4$) was added and thoroughly stirred. 0.2 mol of lanthanum nitrate hexahydrate ($La(NO_3)_3 \cdot 6H_2O$) was then dissolved in the solution before putting into a Teflon-lined, stainless-steel autoclave having a 100 mL capacity. The solution was maintained at 300 °C for 4 h and centrifuged at 6000 rpm. The autoclave was allowed to cool naturally to room temperature while the resulting precipitate was vacuum-dried at 70 °C for two 3 h. The prepared lanthanum erbium telluride ($La_{0.1}Er_{0.2}Te_{0.2}$) nanoparticles were annealed at different temperatures of 500, 550, and 600 °C. Following annealing each nanoparticle, a mixture of 2 mL methanol was added to the nanoparticles to ensure that the particles were blended properly. Subsequently, the film was deposited onto the FTO substrate using the Doctor Blade method (see Figure 1). Once the films were applied onto the substrates, they were allowed to dry completely before being stored for further characterization.

Figure 1. Schematic illustration of the preparation stages of lanthanum erbium telluride ($La_{0.1}Er_{0.2}Te_{0.2}$)

Characterizations

The characterization of the synthesized material was carried out for their structure., morphology, elemental, optical, and electrical properties through the use of Bruker D8 Advance X-ray diffractometer (XRD) with Cu-Kα line (λ =

1.54056 Å), MIRAS TESCAN scanning electron microscope (SEM), Energy dispersive X-ray spectroscope (EDX), 756S UV-Vis Spectrophotometer, and a Four-point probe (Model T345).

Results and discussion

UV spectroscopy study of $La_{0.1}Er_{0.2}Te_{0.2}$ nanoparticle

Figure 2 shows the UV spectroscopy of $La_{0.1}Er_{0.2}Te_{0.2}$ nanoparticles made of hydrothermal and doctor blade deposition. Figure 2 (L1) shows the absorption of light radiation of the synthesized nanomaterial decreasing with wavelength. The $La_{0.1}Er_{0.2}Te_{0.2}$ nanoparticles showed high absorbance in the visible area of the spectra with 0.648 a.u. The absorbance of the material decreased as the annealing temperature increased. The higher the annealing temperature, the lower the absorbance of the material. The unannealed nanoparticle is suitable for light-emitting systems when fabricated. It is ideal for electrodes in batteries, energy storage, solar cells and photovoltaic applications due to its low absorbance. The transmittance of $La_{0.1}Er_{0.2}Te_{0.2}$ nanoparticles in Figure 2 (L2) shows above 80% transmittance for the unannealed material and 68% for the annealed nanoparticle. The transmittance of $La_{0.1}Er_{0.2}Te_{0.2}$ nanoparticles decreased as the annealing temperature increased. The higher the annealing temperature, the lower the transmittance of $La_{0.1}Er_{0.2}Te_{0.2}$ nanoparticles. The nanoparticle had 20% reflectance in the visible region and decreased down the NIN area. However, as the annealing temperature increases, the transmittance decrease and accumulates at a wavelength above 950 nm in Figure 2 (L3). The unannealed nanoparticle has a bandgap energy of 3.50 eV in Figure 2 (L4), and the annealing nanoparticles have a bandgap of 3.27 to 2.26 eV. The higher the annealing temperature, the lower the bandgap of the material.

Structural Study

Figure 3 presents the XRD analysis of nanoparticles with a composition of $La_{0.1}Er_{0.2}Te_{0.2}$. The $La_{0.1}Er_{0.2}Te_{0.2}$ material reveals a hexagonal structure corresponding to a 2theta angle of 13.263°. 15.375°. 16.943°. 18.924°. 25.788°. and 27.356° for $La_{0.1}Er_{0.2}Te_{0.2}$ unannealed and 13.302°. 15.489°. 16.960°. 19.055°. 25.862°. and 27.373° for annealed samples. The material underwent a phase alteration upon annealing at 550°C, resulting in a diffraction peak (111) disappearance at 15.489° 2theta angle. The XRD pattern analysis revealed that the peaks became more distinct as the annealing temperature increased. Based on the data presented in Table 1, it is evident that there is a correlation between the annealing temperature and the crystallite size of $La_{0.1}Er_{0.2}Te_{0.2}$, with an increase in the annealing temperature increasing the size of the crystallites. Equations (1-5) [18,19], [21-27] have been used to calculate some structural characteristics, such as the full width at half maximum (FWHM), crystallite size (D), inter-planar spacing (d), lattice constants, and dislocation density.

$$D = k\lambda / \beta\cos\theta \quad (1)$$

$$d = \lambda / 2\sin\theta \quad (2)$$

$$a = \sqrt{c^2/3} \quad (3)$$

$$c = \lambda/\sin\theta \quad (4)$$

$$\delta = 1/D^2 \quad (5)$$

Table 1 reveals that high temperatures increase average crystallite size with 2theta angles. The annealing temperature was likely affected by nucleation during synthesis. It has also been shown that the distances between the planes and the dislocation density alter when the angle increases. As the atomic radius of $La_{0.1}Er_{0.2}Te_{0.2}$

increases, it can be observed that the lattice angle. constants decrease with an increase in the 2theta

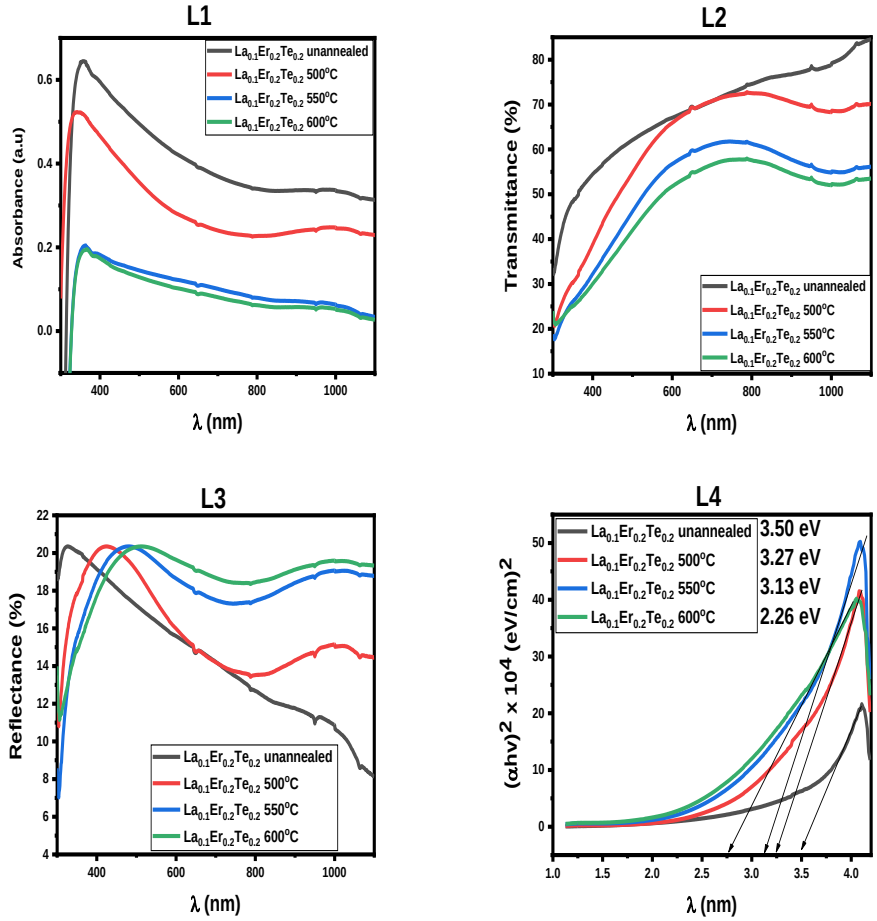

Figure 2. L1-absorbance, L2-transmittance, L3-reflectance, and L4-bandgap energy

Figure 3. XRD pattern of $La_{0.1}Er_{0.2}Te_{0.2}$

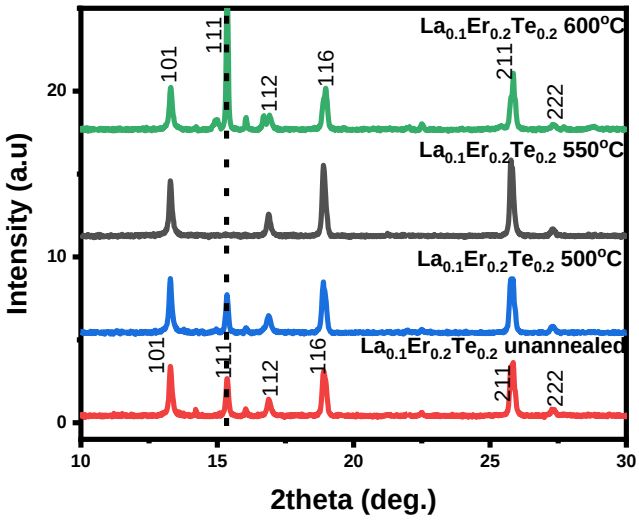

Table 1. $La_{0.1}Er_{0.2}Te_{0.2}$ structural properties **Figure 3.** XRD pattern of $La_{0.1}Er_{0.2}Te_{0.2}$

Films	2θ (deg.)	d (spacing) Å	(Å)	(β)	(hkl)	(D) nm	σ lines/m^2 X 10^{15}
$La_{0.1}Er_{0.2}Te_{0.2}$	13.263	6.6745	11.560	0.2928	101	4.8185	1.3382
	15.375	5.7621	11.524	0.2932	111	4.8484	1.3356
	16.943	5.2322	10.464	0.2934	112	4.7896	1.3323
	18.924	4.6887	10.484	0.2936	116	4.9213	1.3268
	25.786	3.4544	8.4617	0.2938	211	4.9180	1.2975
	27.356	3.2596	9.2197	0.2940	222	4.9146	1.2909
$La_{0.1}Er_{0.2}Te_{0.2}$ 500^{o}C	13.302	6.6550	11.526	0.2748	101	5.1341	1.1786
	15.489	5.7199	11.439	0.2750	111	5.1693	1.1746
	16.961	5.2267	10.453	0.2753	112	5.1045	1.1729
	19.055	4.6568	10.412	0.2755	116	5.2447	1.1678
	25.862	3.4445	8.4372	0.2759	211	5.2371	1.1439
	27.373	3.2577	9.2141	0.2763	222	5.2295	1.1401
$La_{0.1}Er_{0.2}Te_{0.2}$ 550^{o}C	13.302	6.6550	11.526	0.2666	101	5.2920	1.1093
	16.961	5.2267	10.453	0.2672	112	5.2592	1.1049
	19.055	4.6568	10.412	0.2679	116	5.3935	1.1043
	25.862	3.4445	8.4372	0.2681	211	5.3894	1.0801
	27.373	3.2577	9.2141	0.2686	222	5.3794	1.0774
$La_{0.1}Er_{0.2}Te_{0.2}$ 600^{o}C	13.302	5.7199	11.439	0.2487	111	5.6729	9.6538
	15.489	5.2267	10.453	0.2489	112	5.7113	9.6228
	16.961	4.6568	10.412	0.2491	116	5.6414	9.6031
	19.055	3.4445	8.4372	0.2494	211	5.7935	9.5706
	25.862	3.2577	9.2141	0.2498	222	5.7843	9.3775
	27.373	6.6550	11.526	0.2499	101	5.7819	9.3266

Table 2. Electrical Parameters of $La_{0.1}Er_{0.2}Te_{0.2}$

Films	t, (nm)	ρ, (Ω.cm) x 10^4	σ, (S/m) x 10^2
$La_{0.1}Er_{0.2}Te_{0.2}$ unannealed	143.04	67.23	1.48
$La_{0.1}Er_{0.2}Te_{0.2}$ 500^{o}C	146.07	72.64	1.37
$La_{0.1}Er_{0.2}Te_{0.2}$ 550^{o}C	148.09	78.24	1.27
$La_{0.1}Er_{0.2}Te_{0.2}$ 600^{o}C	145.02	81.42	1.22

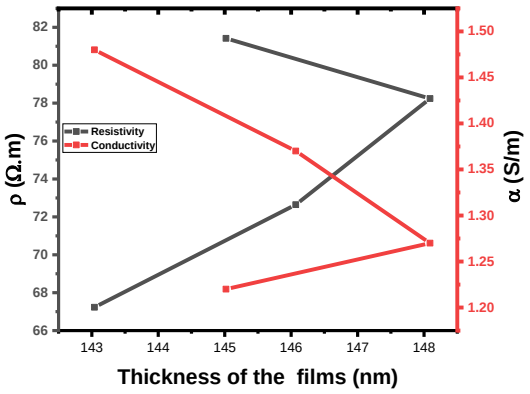

Figure 4. Resistivity and conductivity Vs thickness of the films

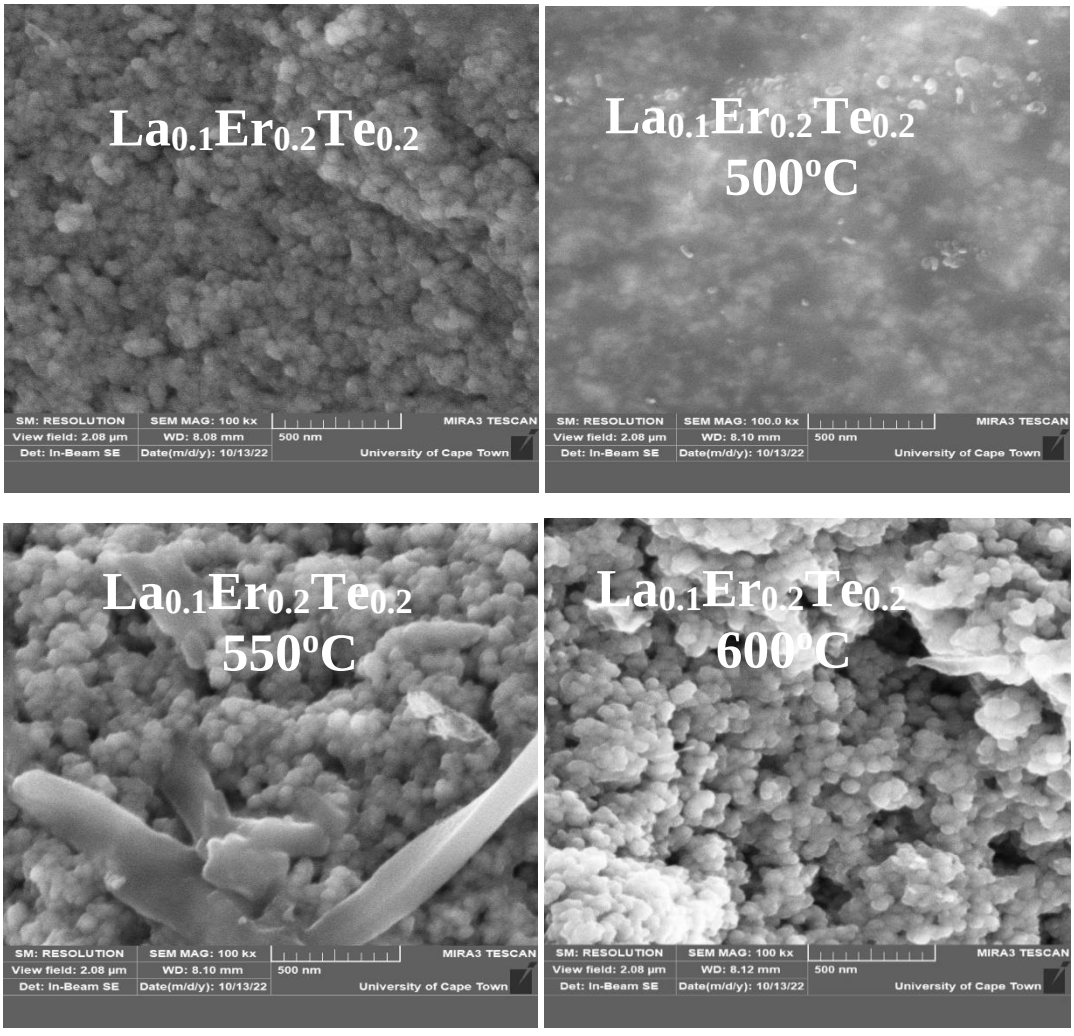

Figure 5. SEM of $La_{0.1}Er_{0.2}Te_{0.2}$

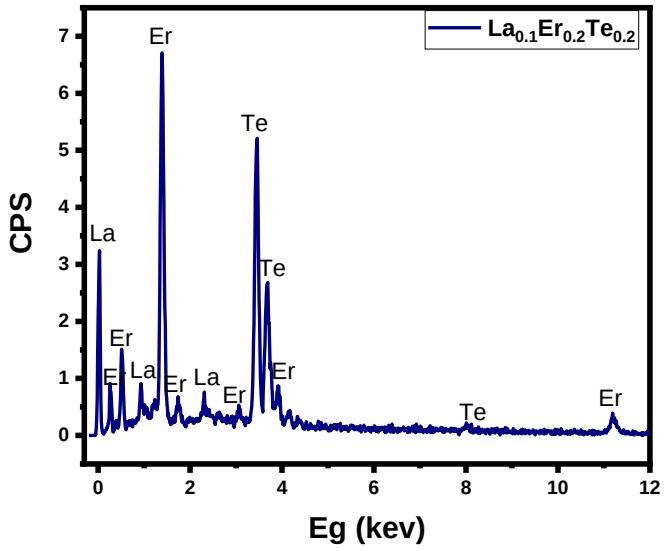

Figure 6. EDXs of $La_{0.1}Er_{0.2}Te_{0.2}$

Resistivity and conductivity study of $La_{0.1}Er_{0.2}Te_{0.2}$

In Figure 4, the relationship between film thickness and both electrical resistivity and conductivity is depicted. As the thickness decreases, the electrical conductivity also decreases in Table 2. In contrast to the previous scenario, the electrical resistivity behavior is exactly the opposite. The annealing temperature decreases electrical conductivity by increasing carrier concentration. This trend allows more electric current to pass through the material, which is beneficial for optoelectronic applications.

Surface morphology of $La_{0.1}Er_{0.2}Te_{0.2}$

Figure 5 shows the surface morphologies of $La_{0.1}Er_{0.2}Te_{0.2}$. Unannealed $La_{0.1}Er_{0.2}Te_{0.2}$ had glow-like nanoparticles. As the annealing temperature rose to 500 ^{o}C, the glow-like nanoparticles decreased.

Conclusions

We have successfully synthesized $La_{0.1}Er_{0.2}Te_{0.2}$ nanoparticles through hydrothermal and doctor blade methods. The $La_{0.1}Er_{0.2}Te_{0.2}$ nanoparticles reveal a hexagonal structure. The XRD pattern showed that the crystallinity increased with higher annealing temperature. Unannealed $La_{0.1}Er_{0.2}Te_{0.2}$ had glow-like nanoparticles. As the annealing temperature rose to 500 ^{o}C, the glow-like nanoparticles decreased. Annealing temperature caused a rise in both nanoparticle clusters and surface energy. The nanoparticles became slightly prone to agglomeration due to temperature. The $La_{0.1}Er_{0.2}Te_{0.2}$ nanoparticles showed high absorbance in the visible area of the spectra with 0.648 a.u. The absorbance of the material decreased as the annealing temperature increased. The higher the annealing temperature, the lower the absorbance of the material. The unannealed nanoparticle has a bandgap energy of 3.50 eV. The annealing nanoparticles have a bandgap of 3.27 to 2.26 eV. The higher the annealing temperature, the lower the bandgap of the material.

Disclosure statement

The authors declare that they have no conflict of interest

Orcid

Imosobomeh L. Ikhioya : 0000-0002-5959-4427

References

[1] A.S. Patil, A.V. Patil, C.G. Dighavkar, V.A. Adole, U.J. Tupe, *Chem. Phys. Lett.*, **2022**, *796*, 139555. [CrossRef], [Google Scholar], [Publisher]

[2] A.C. Nkele, I.L. Ikhioya, E.M. Chigozirim, S.O. Aisid, M. Maaza, F.I. Ezema, *Nanoarchitectonics*, **2020**, 108–114. [CrossRef], [Google Scholar], [Publisher]

[3] V. Balaram, *Geosci. Front.*, **2019**, *10*, 1285–1303. [CrossRef], [Google Scholar], [Publisher]

[4] S. Liang, H. Wang, Y. Li, H. Qin, Z. Luo, B. Huang, X. Zhao, C. Zhao, L. Chen, *Sustain. Energy Fuels*, **2020**, *4*, 3825–3847. [CrossRef], [Google Scholar], [Publisher]

[5] J. Palaparthi, R. Chakrabarti, S. Banerjee, R. Guin, S. Ghosal, S. Agrahari, D. Sengupta, *Arab. J. Geosci.*, **2017**, *10*, 201. [CrossRef], [Google Scholar], [Publisher]

[6] P.C. De Sousa Filho, J.F. Lima, O.A. Serra, *J. Braz. Chem. Soc.*, **2015**, 26, 2471–2495. [CrossRef], [Google Scholar], [Publisher]

[7] Y. Zhong, Z. Chen, F.J. Gonzalez, X. Zheng, G. Li, Y. Luo, A. Mo, A. Xu, S. Wang, *Acta Oceanol. Sin.*, **2018**, *37*, 41–54,. [CrossRef], [Google Scholar], [Publisher]

[8] V. Zepf, *Rare Earth Elements: What and Where They Are* In *Rare Earth Elements*. Springer Theses, Springer, Berlin, Heidelberg. **2013**, pp. 11–39. [CrossRef], [Google Scholar], [Publisher]

[9] H.M. Zakaly, A.S. Abouhaswa, S.A.M. Issa, M.Y. A. Mostafa, M. Pyshkina, R. El-Mallawany, *J. Non. Cryst. Solids*, **2020**, *543*, 120151. [CrossRef], [Google Scholar], [Publisher]

[10] J. Vind, A. Malfliet, B. Blanpain, P.E. Tsakiridis, A.H. Tkaczyk, V. Vassiliadou, D. Panias, *Minerals*, **2018**, *8*, 77. [CrossRef], [Google Scholar], [Publisher]

[11] N. Tepe, M. Romero, M. Bau, *Appl. Geochemistry*, **2014**, *45*, 191–197. [CrossRef], [Google Scholar], [Publisher]

[12] E.L. Payrer, *Light up- conversion in Rare Earth doped Thin Films: Synthesis, Characterization, Luminescence and Prospects for Solar Cell Application*, Doctoral dissertation, Université de Grenoble, Instituto Superieur Tecnico de Lisboa, **2014**. [Google Scholar], [Publisher]

[13] I. Rufus, A. Peter, S.O. Aisida, I.L. Ikhioya, *Results Opt.*, **2023**, *12*, 100464. [CrossRef], [Google Scholar], [Publisher]

[14] S.O. Samuel, M.L.E. Frank, E.P. Ogherohwo, A. Ekpekpo, J.T. Zhimwang, I.L. Ikhioya, *East Eur. J. Phys.*, **2023**, *2023*, 189–196. [CrossRef], [Google Scholar] , [Publisher]

[15] S.O. Samuel, C.K. Ojoba, E.P. Ogherohwo, E.O. Ojegu, J.T. Zhimwang, A. Ekpekpo, I.L. Ikhioya, *J. Indian Chem. Soc.*, **2023**, *100*, 100992. [CrossRef], [Google Scholar], [Publisher]

[16] I. L. Ikhioya, N.I. Akpu, E. Onoh, S.O. Aisida, I. Ahmad, M. Maaza, F. Ezema, *Asian J. Nanosci. Mater.*, **2023**, *2*, 156–167. [CrossRef], [Publisher]

[17] A.C. Nkele, A.C. Nwanya, N.U. Nwankwo, A.B.C. Ekwealor, R.U. Osuji, R. Bucher, M. Maaza, F.I. Ezema, *Mater. Res. Express*, **2019**, *6*, 096439. [CrossRef], [Google Scholar], [Publisher]

[18] F.I Ezema, U.O.A. Nwankwo, *Digest. J. Nanomater. Biostruct.*, **2010**, *5*, 981-988. [Google Scholar]

[19] A.G. Temam, A. Alshoaibi, S.A. Getaneh, C. Awada, A.C. Nwanya, P.M. Ejikeme, F.I. Ezema, *Curr. Opin. Electrochem.*, **2023**, *38*, 101239. [CrossRef], [Google Scholar], [Publisher]

[20] R. Lakra, R. Kumar, D. Nath Thatoi, P. Kumar Sahoo, A. Soam, *Mater. Today: Proc.*, **2021**, *41*, 269–271. [CrossRef], [Google Scholar], [Publisher]

[21] N.N.M. Zorkipli, N.H.M. Kaus, A.A. Mohamad, *Procedia Chem.*, **2016**, *19*, 626–631. [CrossRef], [Google Scholar], [Publisher]

[22] T. Wirunmongkol, N. O-Charoen, S. Pavasupree, *Energy Procedia*, **2013**, *34*, 801–807. [CrossRef], [Google Scholar], [Publisher]

[23] J. T. Chen, J. Wang, R.F. Zhuo, D. Yan, J.J. Feng, F. Zhang, P.X. Yan, *Appl. Surf. Sci*., **2009**, *255*, 3959–3964. [CrossRef], [Google Scholar], [Publisher]

[24] A.S. Golub, Y.V. Zubavichus, Y.L. Slovokhotov, Y.N. Novikov, *Usp. Khim.*, **2003**, *72*, 138–158. [CrossRef], [Google Scholar], [Publisher]

[25] L.F. Jiang, W.Z. Shen, H.Z. Wu, *J. Appl. Phys.*, **2002**, *91*, 9015–9018. [CrossRef], [Google Scholar], [Publisher]

[26] P.A. Lee, G. Said, R. Davis, T.H. Lim, *J. Phys. Chem. Solids*, **1969**, *30*, 2719–2729. [CrossRef], [Google Scholar], [Publisher]

[27] Y. Tian, M. Zheng, Y. Cheng, Z. Yin, J. Jiang, G. Wang, J. Chen, X. Li, J. Qi, X. Zhang, *J. Mater. Chem. C*, **2021**, 9, 13954–13962. [CrossRef], [Google Scholar], [Publisher]

HOW TO CITE THIS ARTICLE

Haneef Shah, Shahbaz Afzal, Mohammad Usman, Kamran Shahzad, Imosobomeh L. Ikhioya *. Impact of annealing temperature on lanthanum erbium telluride ($La_{0.1}Er_{0.2}Te_{0.2}$) nanoparticles synthesized *via* hydrothermal approach, *Adv. J. Chem. A*, **2023**, 6(4), 342-351.

DOI: 10.22034/AJCA.2023.407424.1386
URL: https://www.ajchem-a.com/article_177228.html